Soft Matter

PAPER

View Article Online
View Journal | View Issue

Cite this: *Soft Matter*, 2017, 13, 7381

Influence of multi-cycle loading on the structure and mechanics of marine mussel plaques†

Menaka H. Wilhelm,[ab] Emmanouela Filippidi,[ab] J. Herbert Waite[bcd] and Megan T. Valentine*[ab]

Received 1st July 2017,
Accepted 25th September 2017

DOI: 10.1039/c7sm01299c

rsc.li/soft-matter-journal

The proteinaceous byssal plaque–thread structures created by marine mussels exhibit extraordinary load-bearing capability. Although the nanoscopic protein interactions that support interfacial adhesion are increasingly understood, major mechanistic questions about how mussel plaques maintain toughness on supramolecular scales remain unanswered. This study explores the mechanical properties of whole mussel plaques subjected to repetitive loading cycles, with varied recovery times. Mechanical measurements were complemented with scanning electron microscopy to investigate strain-induced structural changes after yield. Multicyclic loading of plaques decreases their low-strain stiffness and introduces irreversible, strain-dependent plastic damage within the plaque microstructure. However, strain history does not compromise critical strength or maximum extension compared with plaques monotonically loaded to failure. These results suggest that a multiplicity of force transfer mechanisms between the thread and plaque–substrate interface allow the plaque–thread structure to accommodate a wide range of extensions as it continues to bear load. This improved understanding of the mussel system at micron-to-millimeter lengthscales offers strategies for including similar fail-safe mechanisms in the design of soft, tough and resilient synthetic structures.

1. Introduction

In their native intertidal environment, sessile marine mussels, *Mytilus californianus*, routinely contend with crashing waves, tidal ebb and flow, and predators. By depositing a radial array of acellular plaque–tipped threads, called the byssus, each mussel creates its own anchor. Each plaque–thread structure can be viewed as a multicomponent composite: the proximal portion of the thread is shielded within the mussel shell and connects to the exposed distal portion of the thread, which in turn interpenetrates an elliptical, thin-film adhesive plaque.[1] A tough outer cuticle covers the plaque core and distal thread,[2] and the result is a leathery adhesive structure that adheres strongly to a variety of soft and hard substrates.[3]

The remarkable ability of the plaque–thread structure to adhere to wet, fouled, salt-encrusted and corroded surfaces has motivated the study of the interfacial adhesive proteins at the plaque–substrate interface. Such studies have resulted in increasingly comprehensive knowledge of how the mussel foot proteins (mfps) provide hydrogen and metal ion coordination bonding *via* the abundant catecholic side groups of 3,4-dihydroxyphenyl-L-alanine (DOPA), while contributing to cohesive strength by catechol oxidase-mediated protein cross-linking.[4,5] Similarly, the extensibility and self-healing properties[6] of the distal portion of the byssus thread have prompted examination of chemical gradients[7] and metal coordination[8] within the collagen-rich thread. These efforts have improved our knowledge of how dynamic bonding and force-induced bond rupture contribute to toughness at the molecular level.

Despite the crucial role that the plaque plays as an intermediary between the collagen thread and the substrate, the mechanical contributions of the bulk plaque interior are much less understood compared to the interfacial adhesive proteins. Beneath the cuticle coating, the plaque core exhibits a fibre-reinforced cellular structure, consisting of a network of pores[9] with heterogeneous interpenetration of long collagen bundles that connect back to the distal collagen thread. Previously reported fracture toughness of a plaque connected to 2 cm of distal thread,[10] indicated that the system can dissipate energy to provide cohesive strength. Rate-independent mechanical behaviour of adhered plaques[10] measured in the range of 0.6 to 180 μm s^{-1} suggested that supramolecular mechanisms, which function at longer length scales than the previously

[a] *Department of Mechanical Engineering, University of California Santa Barbara, Santa Barbara, CA 93106, USA. E-mail: valentine@engineering.ucsb.edu*
[b] *Materials Research Laboratory, University of California Santa Barbara, Santa Barbara, CA 93106, USA*
[c] *Department of Molecular, Cellular, and Developmental Biology, University of California Santa Barbara, Santa Barbara, CA 93106, USA*
[d] *Biomolecular Science and Engineering Program, University of California Santa Barbara, Santa Barbara, CA 93106, USA*

† Electronic supplementary information (ESI) available. See DOI: 10.1039/c7sm01299c

studied nanoscale molecular bonds, play a role in plaque cohesion and strength. However, the nature of how micro- and mesoscopic mechanisms and structures contribute to cohesive strength and bulk toughening in the plaque is not known.

In order to investigate the origins of cohesive strength and the role of load-induced microscopic changes in the plaque, we examine the effects of repeated loading–unloading cycles on the plaque with a minimal length of thread attached to it ($\sim$2 mm). We employ force–extension curves, which show hysteretic behaviour, and electron microscopy, which shows strain-dependent microstructural changes in the plaque core. Plaque–thread structures subjected to repeated extension exhibit a decrease in small-strain stiffness, which is accompanied by void formation in the porous bulk matrix, slippage at the fibre–foam interface, and fracture of the matrix and/or fibres. Surprisingly, although the plaque sustains several forms of microstructural damage, and in some cases, partial delamination from the underlying substrate, the material strength remains comparable to that of monotonically loaded plaques with no cyclic strain history.

2. Methods

2.1 Mussel plaque collection

Mussels (*Mytilus californianus*; Conrad, 1837) were collected from the fishing pier (34.415605, −119.828911) on the coast of Goleta, CA and placed in shallow tanks with continuously circulated and aerated raw seawater at temperatures ranging from 9 °C to 14 °C. To enable the collection of plaque–thread samples for testing, mussels were tethered *via* large rubber bands to acrylic plates tiled with glass slides (each 75 mm × 25 mm). Every 3–5 days, all plaques deposited onto the glass-slide substrates were collected, following which the mussels were repositioned over fresh slide-coated surfaces to continue their deposition of plaques. Once collected, plaques were rinsed with Milli-Q water and stored at 4 °C for 1–24 days. These studies used a total of 60 plaques harvested from 9 mussels. The plaque-producing mussels were between 8.5–14.5 cm long.

2.2 Mechanical testing

Mechanical testing was performed as previously described.[10] Briefly, a custom-built load frame combines a digital stepper motor, an analogue force sensor, and a microscope for imaging the plaque–glass interface from below. Force, extension, and imaging data were collected at 10 Hz, 20 Hz, and 10 Hz, respectively. Force and extension measurements were down-sampled to 2.5 Hz, by binning measurements from each device in a 0.4 s window and taking their average, to ensure that images are correlated to the force and extension measurements.

To enable secure attachment of the glass-slide-bound plaque to the motor, the thread was glued to a 1 mm diameter glass rod (Sutter Instrument, 415-883-0128) using a polyurethane-based waterproof glue (Gorilla Glue®). A short segment ($\sim$2 mm) of free thread remained between the plaque and rod in all cases. The plaques were left to dry overnight then rehydrated in Milli-Q water for at least 10 minutes before testing. The glass rod was then secured to the motor at an angle of 45° and the plaque was pre-loaded to a measured force of 0.6 N to eliminate slack in the thread. In all cases, a loading rate of 30 μm s^{-1}, or 1.8 mm min^{-1}, was used. For all loading and recovery times, the plaques remained submerged in Milli-Q water. Testing in Milli-Q water, rather than highly oxidative, microorganism-containing seawater, improved experimental repeatability.

Previous work showed that plaque detachment force scaled linearly with plaque diameter D_p.[10] The geometric mean of the diameters of the elliptical plaque's major-dimension (D_M) and minor-dimension (D_m) was calculated as follows: $D_p = \sqrt{D_M \times D_m}$. This allowed the measured detachment force F to be normalized to account for variations in plaque diameters: $F^* = F \times (2.5\ \text{mm}/D_p)$ where 2.5 mm was the mean diameter of all plaques tested. Total length of the thread for each sample was controlled to be 2 mm, and extension was not normalized.

Samples were monotonically loaded until failure. As is common in soft-materials testing, many samples failed due to stress concentrations associated with gluing the end of the thread. Samples that failed at the plaque typically failed by loss of adhesion at the plaque–glass interface, although internal cohesive failure was also sometimes observed, in agreement with prior studies.[10] We included all failure modes in our analysis, and statistical analysis of the ultimate stresses associated with each failure showed no statistical differences between them (Table S1, ESI†).

Cyclic tests were informed by the yield observed in monotonic tests. The approach to yield was monitored through calculation of the force difference measured between successive motor steps. In cyclic loading, plaques were first pulled until this force difference dropped below a threshold set to 5 mN, indicating exit from the linear response regime. We call the extension corresponding to this force threshold Δx_y. The plaques were then unloaded fully, and pulled to $2\Delta x_y$ then unloaded to zero extension again, and pulled next to $4\Delta x_y$. In the fourth and final cycle, the plaques were loaded to failure (Table 1). All cyclic tests were extension-controlled.

2.3 Force–displacement curve analysis

To determine the extent of the initial linear elastic range, we used a custom-written, semi-automated fitting routine implemented in MATLAB. For each loading curve, the fit was manually initialized with two inputs: the maximum range of extensions over which the force–displacement F–Δx data should be fit, and one anchor point that must be included in the final fit. The program then iteratively performed linear fits over all possible ranges of points that included the anchor

Table 1 Extension sequence of loading–unloading cycles

Cycle	1	2	3	4
Loaded to	Yield, Δx_y	$2\Delta x_y$	$4\Delta x_y$	Failure
Unloaded to	Zero extension			None

point within the maximum range. Any range containing less than 2 s of measured data was discarded. Of the ranges that contained sufficient data, we selected the range with maximum *R*-squared value, and used this as the final linear fit. The linear fits were not forced through zero, and the zero-force extension (*x*-intercept) of the final fit was subtracted from the extension data. To determine the transition between linear loading and non-linear yield, we compared the expected force value predicted from the fit to the measured force at each extension. We defined the proportional limit threshold as the point where the difference between the expected and measured force values exceeded 5 mN. The proportional limit has associated extension, Δx_{PL}, and force, F_{PL}. F_{PL} was approximately 1 N for all specimens.

2.4 Scanning electron microscopy

Scanning electron microscopy (SEM) was used to image the internal structures of the mussel plaques, as previously described.[9] Briefly, plaques were fixed for 4 hours in a solution of 3.7% formaldehyde and 2.5% glutaraldehyde in water. Following fixation, the plaques were stored in Milli-Q water at 4 °C for 1–3 days. Each plaque was then embedded in Neg-50 cryoprotectant (Thermo Scientific) and sectioned at −21 °C (Leica CM 1850) to create 20 μm thick slices parallel to the direction of the thread (along the long axis of the elliptical plaque) that were immediately placed in Milli-Q water. All sections were rinsed repeatedly to remove cryoprotectant, then taken through several rounds of solvent exchange from water to ethanol using ratios of water : ethanol as follows: 3 : 1, 1 : 1, 1 : 3, 1 : 9, 0 : 1. Sections were rinsed three times with ethanol to ensure no water remained, then exchanged from ethanol to hexamethyldisilazane (HMDS, CAS 999-97-3) using ratios of ethanol : HMDS of 2 : 1, 3 : 2, 1 : 2. Samples were mounted on aluminum microscopy stubs using carbon adhesive, and sputter coated for 90 s with gold/palladium 60/40 99.99% (Hummer 6.2, Anatech, USA). Imaging was performed with the FEI Nova NanoSEM at an accelerating voltage of 5 kV. Experiments for each condition were performed in triplicate.

3. Results

3.1 Monotonic loading to failure

Monotonically-loaded plaque–thread samples pulled at a 45° angle and 30 μm s^{-1} loading rate exhibited an overall similar response: an initial elastic regime followed by a yield region and an eventual increase in force at extensions comparable to or exceeding the unloaded thread length (Fig. 1). Although the individual mussel age and size influenced the plaque properties, we found that scaling by the plaque's geometric mean, D_p, and normalizing by the proportional limit, F_{PL}, collapsed the data and allowed for comparison among different mussel samples.

The irregular and variable geometry of the plaque–thread samples prevented the straightforward conversion of our mechanical data, which is collected as force and extension as functions of time, to stress and strain. Thus, the small-displacement stiffness was determined from a linear fit of the force–displacement curve

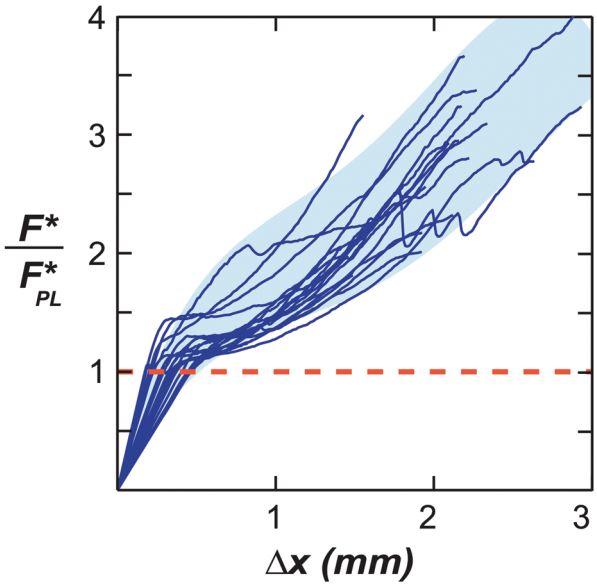

Fig. 1 Force required to extend the plaque–thread sample in monotonic loading. The force response for individual plaque–thread samples varies among different mussels, but the curves largely collapse when normalized by the proportional limit of force F_{PL} (number of plaques, n = 18, derived from 9 different mussels). Each curve displays the same general features: an initial linear regime, followed by a yield region, and an eventual increase in force at large extensions. The dotted line at $F^*/F_{PL}^* = 1$ indicates the transition from the linear regime to the yield region for each sample. The shaded area indicates the range of the monotonic loading data. This range was created by manually selecting points to create maximum and minimum bounds of the envelope, then fitting these respective series of points to a 4th order polynomial function. Original data without scaling by F_{PL} are shown in Fig. S1 (ESI†).

with a maximum linear extension that did not exceed 0.3 mm. Given our thread length of ~2 mm and the low height profile of the adhered plaque (100–200 μm), we estimate that this value corresponds to approximately 10% strain in the structure. The linear stiffness serves as a proxy for the elastic modulus, and the maximum force measured for a given loading cycle is interpreted as the sample strength.

One important difference between the current study and previous mechanical tests of adhered plaques is a reduction in the length of the exposed thread that is allowed to contribute to load transmission, from 20 mm in prior work[10] to 2 mm here. Interestingly, in both cases, similar force responses and failure modes were observed. The onset of yield occurred at extensions of ~0.2 mm, or ~10% of the total thread length and the forces, F_y, associated with this yield ranged from 0.25 N to 1.5 N. Structural failure or detachment occurred at extensions of ~0.6 mm–1 cm, or ~30–50% of total thread length in the case of the 2 cm long thread and at extensions of ~2 mm, or ~100% of thread length for the 2 mm length thread. Maximum forces were extremely similar, ranging from 1 N to 4 N in the 2 cm thread case and from 0.5 N to 3 N in the 2 mm thread case, despite the 10-fold reduction in thread length. This suggests some role for the plaque in determining the critical extension and force at failure, independent of the thread length. It is possible that chemical gradients within the thread[7] play a role,

resulting in stronger contributions to load-bearing in the portion of the thread closest to the plaque. Also, whereas in the previous study the thread was partially hydrated by misting during the measurement, in this study it was completely submerged. Furthermore, a preparation step of drying, gluing to a rod, and rehydrating was added to this study. As the mussel thread and plaque naturally encounter drying and rehydration in the intertidal zone,[11] we expect any effects due to drying to be minimal.

3.2 Mechanics of multi-cycle loading

The response of plaque–thread structures to multi-cyclic loading was investigated using the extension-controlled cyclical scheme 1 described in Table 1, resulting in similar overall mechanical responses. Cyclic loading within the linear regime resulted in reversible unloading–loading behaviour with minimal hysteresis (data not shown). However, for each cycle that loaded the plaque–thread into the yield domain, we observed hysteresis (Fig. 2) between the loading and unloading curves. For all cycles, unloading occurs along a unique slope, which differs from that of the previous loading, as well as that of the subsequent reloading; in each case the value of the force when the sample is fully unloaded approaches zero. The dissipated energy, which can be approximated by the enclosed area within the hysteretic loop, increased with each loading cycle to greater extension. The sample stiffness, K, which was determined from the initial slope of the F–Δx curve for each cycle, decreased with subsequent loading, indicating that at least some of the observed toughening arises from irreversible plastic mechanisms that compromise the small-strain elasticity (Fig. 3). We observed a modest stiffness decrease of K_2 by $\sim$10% relative to K_1. When the samples were extended further into the non-linear regime in cycles 3 and 4, the stiffness decreased further. By the third loading K_3 was typically reduced to $\sim 0.5K_1$, and by cycle 4, K_4 was only $\sim 0.2K_1$.

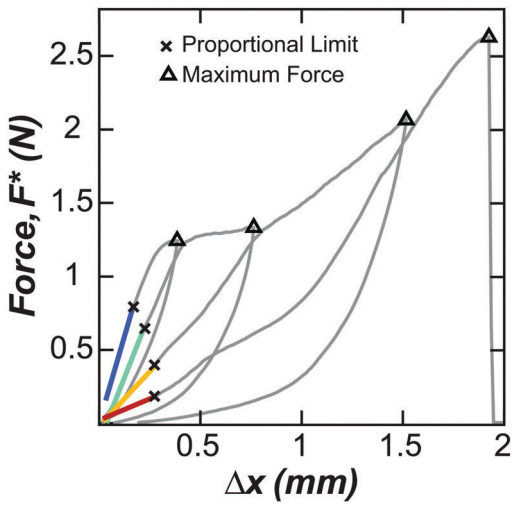

Fig. 2 The force–extension curve for a representative cyclic loading experiment. The small-strain stiffness fit for each loading curve is shown in a different color (cycle 1 in blue, cycle 2 in cyan, cycle 3 in gold, and the final load to failure in red). For each cycle the peak force (open triangles) and the proportional limit (X-mark) is shown. No recovery time was allowed in between unloading and loading cycles for this trace.

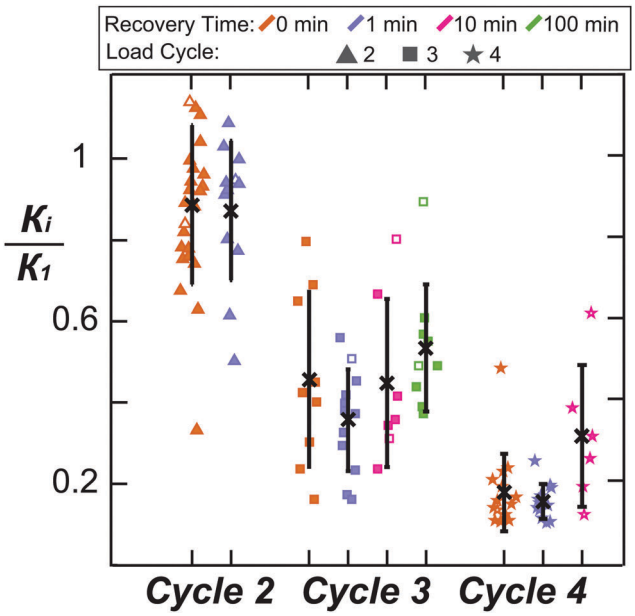

Fig. 3 The change in small-strain stiffness as a function of recovery time and cycle. Here, the change in small-strain stiffness is calculated as the ratio of the stiffness measured during the i-th loading cycle (K_i) to the initial small-strain stiffness (K_1), measured during the first loading. Different colours show varying recovery times between the shown stiffness and the previous load cycle. The data points are slightly offset along the x-axis to improve readability. In all cases, the measured stiffness decreases when subjected to additional loading cycles, so the value is always <1. No strong evidence of recovery is found. An open symbol denotes a plaque that was partially delaminated at the proportional limit of the loading cycle; delamination appears to have little effect on the small-strain stiffness.

The nonlinear F–Δx response also depended on the previously applied maximum extension. For applied extensions exceeding the maximum of the previous cycles, the force extension response upon loading closely resembled that of pristine samples that were monotonically loaded to failure. In contrast, for extensions that were less than the previous maximum value, the force response was consistently lower than that measured in the initial pull, but higher than the forces developed in the prior unloading. Such dependence of the nonlinear mechanical response on the prior loading history is common in a wide range of polymeric samples, including elastomers[12] and hydrogels.[13] However, in contrast to the classic Mullins effect,[14] the reloading curves do not follow the previous unloading curve exactly, indicating some level of recovery when the pulling force is reduced.

3.3 Time-dependent recovery of mussel plaque mechanics

To further explore the ability of loaded mussel plaque–thread systems to recover their mechanical strength and properties after loading, we repeated the multi-cycle loading experiments using three additional loading schemes #2–#4 presented in Table 2, with varying recovery times in between cycles. In all cases, we found the same general features as those observed with no recovery time between any of the cycles (scheme #1).

Table 2 Recovery times for loading schemes

	Recovery time between cycles		
	1 and 2	2 and 3	3 and 4
Scheme #1	0 min	0 min	0 min
Scheme #2	1 min	1 min	1 min
Scheme #3	0 min	10 min	10 min
Scheme #4	0 min	100 min	0 min

For example, the stiffness in cycle i, K_i, was statistically independent of the recovery time between cycles and no evidence of significant stiffness recovery for recovery times of up to 100 minutes was observed (Fig. 3, green markers). Interestingly, we did not observe a difference in the stiffness reduction between plaques that were fully adhered to the glass surface and plaques that had started to delaminate (compare solid and open symbols in Fig. 3). This may suggest that K is dominated by bulk effects, rather than the mechanics and load transfer properties of the interface.

To investigate how this repetitive loading affected plaque strength, we superimposed the normalized peak force measured from each loading cycle on the normalized range of force responses from plaques loaded monotonically (Fig. 4). In most cases, progressive peak forces continued to rise in a manner that closely resembled the stiffening observed in the monotonic force response. Samples loaded with no recovery time still exhibited peak forces coinciding with the range of force response in pristine samples, as did those with longer recovery times (compare different colours, Fig. 4). Additionally, plaques showing partial delamination at the measured peak force maintained strength comparable to fully adhered samples (open symbols, Fig. 4), suggesting that the strength of the plaque–thread structure is not affected by cyclic load history, nor even partial delamination.

3.4 Microscale damage in plaques subjected to large deformations

The core and exterior of plaques were observed by SEM to study the effect of the various extensions on the microstructure, and in particular to pinpoint the onset of microstructural damage. In control plaques that were not subjected to loading, the core of the plaque showed a cohesive porous network structure (Fig. 5), with collagen thread interpenetration evident as darker bands throughout the foam (plum ellipse), consistent with prior results.[9] At the internal interfaces where the foam meets the collagen thread, these two materials appeared completely connected (Fig. 5A, light blue ellipse). Some amount of pore compression was evident within the bulk, particularly near the interface between the substrate and foam, but no damage was evident (Fig. 5D, light green).

At $2\Delta x_y$ extension, where the largest decrease in stiffness per applied elongation was observed, the external integrity of the plaque was not compromised. However, significant microstructural damage was evident at the plaque core (Fig. 6).

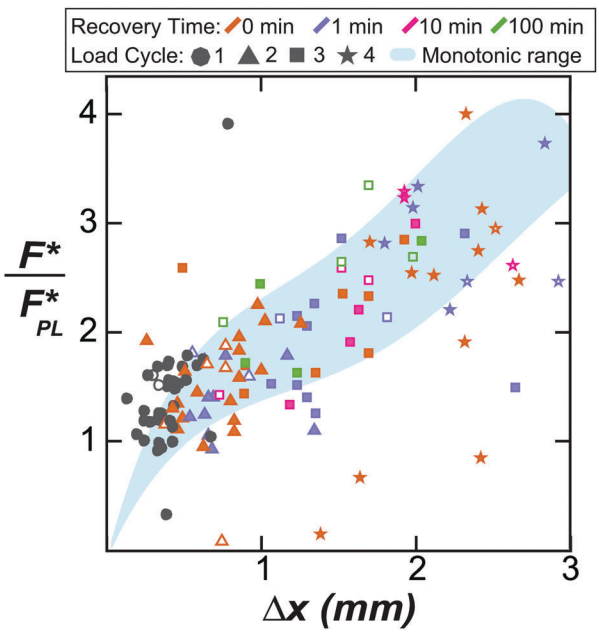

Fig. 4 Peak forces measured in cyclic tests follow the monotonic loading curve, independent of load history and delamination. Here, the peak forces from all cyclic loading tests are compared with the range of monotonic force response. Different colors show the peak forces of loading cycles with different recovery times (no recovery time in orange, 1 min recovery time between each cycle in purple, 10 minutes recovery time between cycles 2 and 3 in pink, and 100 minutes recovery time between cycles 2 and 3 in green). Different shapes denote the loading cycle from which the peak force was extracted, as described in the inset. Open symbols show samples which were partially delaminated at the peak force measurement.

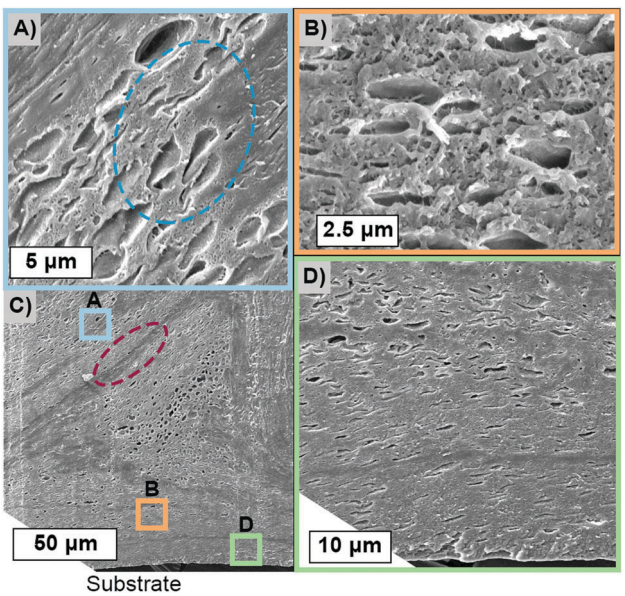

Fig. 5 Internal microstructure of unstrained plaque. Plaque is sectioned parallel to the direction of the distal thread, and lower left inset, (C), shows whole-section view of respective samples. Dashed plum ellipse highlights where collagen interpenetrates the foamy structure. Three regions are shown at higher magnification to allow microscale features to be more easily observed: (A) the thread–foam interface is intact (light blue dashed ellipse). (B) The foam structure in the unstrained bulk shows pores with two length-scales. (D) Foam at the substrate edge is intact, and pores show some compression from circular entities to elliptical entities.

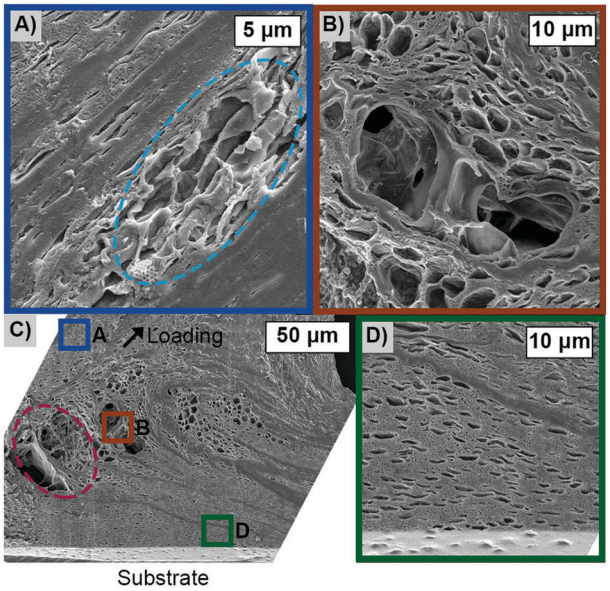

Fig. 6 Internal microstructure of plaque strained to $2\Delta x_y$. Plaque is sectioned parallel to the direction of the distal thread, and lower left inset (C) shows whole section view of respective samples. Dashed plum ellipse highlights where collagen interpenetrates the foamy structure. Three regions are shown at higher magnification to allow microscale features to be more easily observed: (A) delamination between the collagen thread and porous foam appears at the highest point of the foam (dashed blue ellipse). (B) Large voids form in the porous structure. (D) In this case, the interface remains intact.

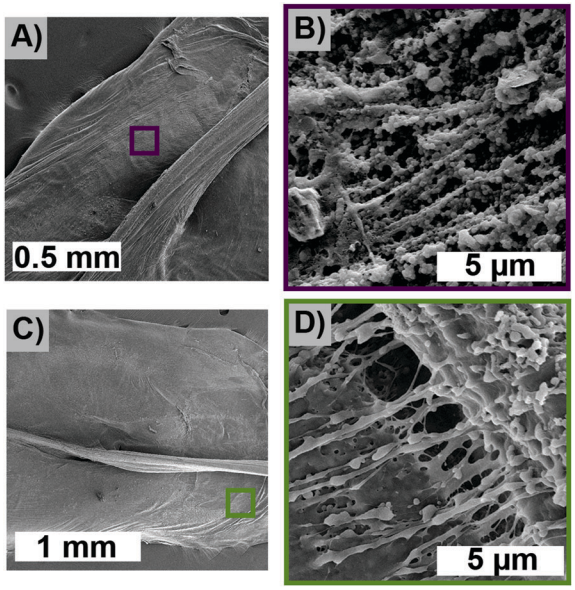

Fig. 7 External microstructure of unstrained plaque compared to plaque strained to $4\Delta x_y$. (A) Whole plaque–thread structure of unstrained plaque, view from above. (B) Bands of cuticle granules appear dense and undamaged. (C) Whole plaque–thread structure strained to $4\Delta x_y$. (D) Fibrils thin and stretch apart under strain.

The fibrous network of collagen fibres appeared to have been pulled apart in some areas (Fig. 6, plum ellipse), and delamination occurred at the collagen fibre–foam interface (Fig. 6A, blue ellipse). In addition, large voids ripped open in the porous core (Fig. 6B). Despite these structural changes, the porous foam at the plaque:-substrate interface remained unchanged (Fig. 6D), although this varied from sample to sample. In some mechanical tests delamination of plaques at similar extensions was observed. Plaques pulled to an extension of $2\Delta x_y$ and allowed to recover for 100 minutes before imaging still exhibited many of the same microstructural changes evident in plaques fixed at strain with no recovery. The existence of large scale, irreversible structural damage is consistent with the observed reduction of small-strain stiffness with each loading cycle, and the lack of stiffness recovery (for at least 100 minutes of recovery time) (Fig. 3).

Finally, at even higher extensions of $4\Delta x_y$, where $K_3 \sim 0.2K_1$, external microstructural damage was observed (Fig. 7). Plaques extended to $4\Delta x_y$ exhibited separation and thinning of bands of granules of the cuticle coating, which extends from the thread over much of the plaque.

4. Discussion

In monotonic loading, the plaque–thread materials performed robustly and consistently, as shown in Fig. 1. Agreement among samples from different mussels is particularly interesting, considering the variability in material processing of these structures. Even among plaques deposited by the same individual mussel, protein polymorphism likely causes differences in plaque protein compositions.[15] Plaque size and proportions of plaque constituents (*i.e.* height of foamy core, thickness of cuticle) vary, and although the time between plaque deposition and collection was reasonably controlled, some plaques necessarily had longer exposure to seawater before collection than others. The mussel thus creates a strong material without controlling every material parameter at a minute level. In addition to reconciling material variability, the plaque–thread structure also accommodates internal damage and even partial delamination of the plaque from the substrate, while maintaining its strength at large extensions.

Upon repeated loading, energy is dissipated as microscale tears and voids form within the disordered core foam and the foam–thread interface experiences disruption. In some cases, a disc-shaped crack between the plaque and the substrate forms and begins to propagate. The presence of such damage compromises small-strain stiffness, but does not affect material strength, suggesting the existence of multiple force transmission pathways between the thread and plaque–substrate interface, where some pathways retain integrity at intermediate forces. Thus, in addition to distributing load between an array of threads, the byssus may evade failure by incorporating multiple, nested sacrificial networks that are called to bear load only when needed. Such strategies have been identified in other biological materials,[16] and have been exploited in synthetics, most notably in double network hydrogels[17] and elastomers.[12] The incorporation of such fail-safe dissipative mechanisms would allow damage to be accommodated without catastrophic failure, possibly in similar fashion to the granular

cuticle which surrounds both plaque and thread and exhibits microcracking before thread rupture. The ability of the structure to maintain strength despite plaque–substrate delamination may also arise from mechanically-induced chemical reactions within the plaque that help to compensate for structural damage, similarly to what has been suggested to occur at the plaque interface.[18] Other chemical properties that could contribute to the observed robustness include the antioxidant ability of mfp-6[19] which results in the maintenance of the reducing environment at the interface for many weeks.[20] Finally, at large extensions, load transfer through the thread and plaque results in microstructural damage at the thread–foam interface. This damage, which occurs within the collagen fibres and the surrounding foam matrix, suggests a mechanical mismatch between the thread and foam core. Because damage to this thread–foam interface precedes damage detected at the cuticle-collagen matrix, it is likely that the thread–foam mismatch exceeds the mechanical mismatch between the cuticle and collagen. This suggests that the foamy core may play an important role in toughening, while the cuticle-interior interface contributes primarily to load-bearing and strength.

The mechanical behaviour we observed in plaque–thread structures shares character with measurements of the collagenous distal thread alone, which exhibits a high initial stiffness before yield, occurring at 10–20% strain, then a plateau and final stiffening beyond yield, in qualitative agreement with our results.[21] Similarly, in cyclic loading, the distal thread also exhibits stress softening and dissipative hysteresis that increases with increasing extension.[6] This similarity is perhaps not surprising, since in our experiments, the thread interpenetrates the plaque and accounts for 90% of the total length of the structure. However, the recovery exhibited by distal threads[8] contrasts with our results. Although we do observe some level of immediate recovery in cyclic loading, as progressive cycles consistently result in higher forces than are observed at the same strain in the unloading of the previous cycle, we do not observe appreciable recovery in small-strain stiffness at timescales up to 100 minutes. These differences suggest that, unlike the thread, the plaque contributes toughening by dissipating applied stress in progressive plastic deformation. The strain rate used in our experiments, 30 μm s^{-1}, corresponds to quasi-static conditions, that are most probably under-estimating the naturally-occurring strain rates. Carrington and Gosline[6] perform their experiments in the rate range of 80–420 μm s^{-1}, and even report experiments at 16 666 μm s^{-1}, which are closer to the naturally-occurring strain rates, as the mussels are subjected to waves with speeds up to 10 m s^{-1}.[22]

Man-made foams designed for structural applications are typically used in compression to enhance energy dissipation through controlled structural collapse, or to increase stiffness without substantially increasing mass.[23] In contrast, the foam within the mussel plaque is more likely subjected to tension and/or shear. The behaviour of closed cell polymeric foams in tension is dominated by bending of cell walls,[24] which may occur in the larger, closed pores evident within the mussel plaque foam, but the role of the surrounding network of smaller, open pores is less clear.[9] Within the foam matrix, we observed crack propagation through pore centres suggesting that pore rupture can advance fracture. However, ductile or semi-ductile behaviour within the foam matrix and matrix porosity could also contribute to crack tip blunting, discouraging crack advance.[25] The disordered existence of heterogeneous material boundaries within the plaque–thread structure (between foam and water, or foam and thread, for example) may also reduce opportunities for linear crack advance, as has been proposed in another porous, non-mineralized biomaterial, squid sucker rings.[26]

5. Conclusions

The mussel plaque–thread structure leverages multiscale, multi-phase structural components to support required loads even after damage occurs. As soft materials are increasingly candidates in multi-faceted functions, such as stretchable electronics, the design of materials with multiple routes to resiliency is essential. Translating this strategy to implement a multiplicity of load-bearing strategies in synthetic materials holds potential for creating new classes of soft, yet strong, architectured materials.

Conflicts of interest

There are no conflicts to declare.

Acknowledgements

Authors thank Robert McMeeking and Daniel DeMartini for useful discussions and Mark Cornish for technical assistance. This work was supported by the MRSEC Program of the National Science Foundation under Award No. DMR 1121053. JHW acknowledges partial support from the National Institutes of Health Grant R01-DE018468. Use of the Shared Experimental Facilities of the Materials Research Science and Engineering Center at UCSB (MRSEC NSF DMR 1121053) is gratefully acknowledged. The UCSB MRSEC is a member of the NSF-supported Materials Research Facilities Network (www.mrfn.org).

References

1 D. J. Crisp, G. Walker, G. A. Young and A. B. Yule, *J. Colloid Interface Sci.*, 1985, **104**, 40–50.
2 N. Holten-Andersen, T. E. Mates, M. S. Toprak, G. D. Stucky, F. W. Zok and J. H. Waite, *Langmuir*, 2009, **25**, 3323–3326.
3 J. H. Waite, *Int. J. Adhes. Adhes.*, 1987, **7**, 9–14.
4 L. M. McDowell, L. A. Burzio, J. H. Waite and J. Schaefer, *J. Biol. Chem.*, 1999, **274**, 20293–20295.
5 B. P. Lee, P. B. Messersmith, J. N. Israelachvili and J. H. Waite, *Annu. Rev. Mater. Res.*, 2011, **41**, 99–132.
6 E. Carrington and J. Gosline, *Am. Malacol. Bull.*, 2004, **18**, 135–142.
7 C. Sun and J. H. Waite, *J. Biol. Chem.*, 2005, **280**, 39332–39336.
8 C. N. Z. Schmitt, Y. Politi, A. Reinecke and M. J. Harrington, *Biomacromolecules*, 2015, **16**, 2852–2861.

9 E. Filippidi, D. G. DeMartini, P. Malo de Molina, E. W. Danner, J. Kim, M. E. Helgeson, J. H. Waite and M. T. Valentine, *J. R. Soc., Interface*, 2015, **12**, 20150827.
10 K. W. Desmond, N. A. Zacchia, J. H. Waite and M. T. Valentine, *Soft Matter*, 2015, **11**, 6832–6839.
11 M. W. Denny and R. T. Paine, *Biol. Bull.*, 1998, **194**, 108–115.
12 E. Ducrot, Y. Chen, M. Bulters, R. P. Sijbesma and C. Creton, *Science*, 2014, **344**, 186–189.
13 R. E. Webber, C. Creton, H. R. Brown and J. P. Gong, *Macromolecules*, 2007, **40**, 2919–2927.
14 L. Mullins, *Rubber Chem. Technol.*, 1969, **42**, 339–362.
15 S. C. Warner and J. H. Waite, *Mar. Biol.*, 1999, **134**, 729–734.
16 G. E. Fantner, E. Oroudjev, G. Schitter, L. S. Golde, P. Thurner, M. M. Finch, P. Turner, T. Gutsmann, D. E. Morse, H. Hansma and P. K. Hansma, *Biophys. J.*, 2006, **90**, 1411–1418.
17 J. P. Gong, Y. Katsuyama, T. Kurokawa and Y. Osada, *Adv. Mater.*, 2003, **15**, 1155–1158.
18 J. H. Waite, *J. Exp. Biol.*, 2017, **220**, 517.
19 J. Yu, W. Wei, E. Danner, R. K. Ashley, J. N. Israelachvili and J. H. Waite, *Nat. Chem. Biol.*, 2011, **7**, 588–590.
20 D. R. Miller, J. E. Spahn and J. H. Waite, *J. R. Soc., Interface*, 2015, **12**, 20150614.
21 E. C. Bell and J. M. Gosline, *J. Exp. Biol.*, 1996, **199**, 1005–1017.
22 M. Denny, B. Gaylord, B. Helmuth and T. Daniel, *Limnol. Oceanogr.*, 1998, **43**, 955–968.
23 B. H. Smith, S. Szyniszewski, J. F. Hajjar, B. W. Schafer and S. R. Arwade, *J. Constr. Steel Res.*, 2012, **71**, 1–10.
24 V. S. Deshpande and N. A. Fleck, *Acta Mater.*, 2001, **49**, 1859–1866.
25 R. M. McMeeking, *J. Mech. Phys. Solids*, 1977, **25**, 357–381.
26 A. Miserez, J. C. Weaver, P. B. Pedersen, T. Schneeberk, R. T. Hanlon, D. Kisailus and H. Birkedal, *Adv. Mater.*, 2009, **21**, 401–406.

